

Velocity and stress autocorrelation decay in isothermal dissipative particle dynamics

Anuj Chaudhri and Jennifer R. Lukes*

Department of Mechanical Engineering and Applied Mechanics, University of Pennsylvania, Philadelphia, Pennsylvania 19104, USA

(Received 8 December 2008; revised manuscript received 2 November 2009; published 19 February 2010)

The velocity and stress autocorrelation decay in a dissipative particle dynamics ideal fluid model is analyzed in this paper. The autocorrelation functions are calculated at three different friction parameters and three different time steps using the well-known Groot/Warren algorithm and newer algorithms including self-consistent leap-frog, self-consistent velocity Verlet and Shardlow first and second order integrators. At low friction values, the velocity autocorrelation function decays exponentially at short times, shows slower-than exponential decay at intermediate times, and approaches zero at long times for all five integrators. As friction value increases, the deviation from exponential behavior occurs earlier and is more pronounced. At small time steps, all the integrators give identical decay profiles. As time step increases, there are qualitative and quantitative differences between the integrators. The stress correlation behavior is markedly different for the algorithms. The self-consistent velocity Verlet and the Shardlow algorithms show very similar stress autocorrelation decay with change in friction parameter, whereas the Groot/Warren and leap-frog schemes show variations at higher friction factors. Diffusion coefficients and shear viscosities are calculated using Green-Kubo integration of the velocity and stress autocorrelation functions. The diffusion coefficients match well-known theoretical results at low friction limits. Although the stress autocorrelation function is different for each integrator, fluctuates rapidly, and gives poor statistics for most of the cases, the calculated shear viscosities still fall within range of theoretical predictions and nonequilibrium studies.

DOI: [10.1103/PhysRevE.81.026707](https://doi.org/10.1103/PhysRevE.81.026707)

PACS number(s): 47.11.-j, 66.20.Cy

I. INTRODUCTION

Dissipative particle dynamics (DPD) is a meshless, coarse-grained, particle-based mesoscopic method that has been used to model complex fluid systems such as lipid bilayer membranes, vesicles, micelles, binary immiscible fluids, suspensions, composites, and polymersomes [1,2]. The equations of DPD are stochastic differential equations with conservative, dissipative and random forces. The key component of DPD is Eq. (1), which advances the DPD particle (“bead”) velocities over time by the action of three separate forces

$$\mathbf{F}_i = \mathbf{F}_i^C + \mathbf{F}_i^D + \mathbf{F}_i^R. \quad (1)$$

The conservative (\mathbf{F}^C), random (\mathbf{F}^R), and dissipative (\mathbf{F}^D) forces depend on position and the dissipative forces additionally depend on the velocities of the interacting pairs of beads. The dissipative and random force contributions to the total force in Eq. (1) are given by [3,4]

$$\mathbf{F}_i^D = \sum_{j \neq i} -\gamma_{ij} [w_{ij}^D(\mathbf{r}_{ij})] [\mathbf{v}_{ij} \cdot \hat{\mathbf{r}}_{ij}] \hat{\mathbf{r}}_{ij}, \quad (2)$$

$$\mathbf{F}_i^R = \sum_{j \neq i} \sqrt{2\gamma_{ij} k_B T w_{ij}^R(\mathbf{r}_{ij})} \psi_{ij} dt^{-1/2} \hat{\mathbf{r}}_{ij}, \quad (3)$$

where w_{ij}^D, w_{ij}^R are arbitrary weight functions, γ_{ij} is the dissipative (friction) parameter between particles i and j , ψ_{ij} is a normal random number of zero mean and unit variance, and the i_j^{th} velocity and dimensionless position vectors are defined as

$$\mathbf{v}_{ij} = \mathbf{v}_i - \mathbf{v}_j, \quad (4)$$

$$\hat{\mathbf{r}}_{ij} = \frac{\mathbf{r}_i - \mathbf{r}_j}{|\mathbf{r}_i - \mathbf{r}_j|} = \frac{\mathbf{r}_i - \mathbf{r}_j}{|\mathbf{r}_{ij}|}. \quad (5)$$

The conservative force is usually chosen as soft repulsive as proposed by Groot and Warren in [5].

$$\mathbf{F}_i^C = \sum_{j \neq i} a_{ij} w_{ij}^C(\mathbf{r}_{ij}) \hat{\mathbf{r}}_{ij}. \quad (6)$$

Here, a_{ij} represents the strength of the conservative force, and $w_{ij}^C(\mathbf{r}_{ij})$ is a weight function for the conservative force. The exact expressions for the dimensionless equations and their scaling factors can be found in Ref. [6].

The dissipative and random force parameters are constrained to satisfy the fluctuation-dissipation theorem [3], and hence act as a thermostat in the process. The conservative forces as defined by Groot and Warren are phenomenological in nature. However, it has been suggested that the method is more general and is not limited to the Groot/Warren model only [7]. The method can be thought of as a “DPD thermostat” where the conservative forces are either phenomenological (Groot/Warren model) or can be derived from atomistic or mean-field description of the system [7].

Previous studies [5,8–11] have shown that properties such as temperature, radial distribution function, and tracer diffusion coefficient for ideal fluids are strongly dependent on the time step and on the choice of dissipative and random force parameters (Table I) used to calculate (\mathbf{F}^D) and (\mathbf{F}^R). A major obstacle to the improvement of such algorithms is the stochastic nature of the DPD equations. Although numerical integration techniques for ordinary differential equations are well established [12], analogous techniques for stochastic ordinary differential equations are still an active area of re-

*jrlukes@seas.upenn.edu

TABLE I. Values of dimensionless DPD parameters used in the 3D simulations.

PARAMETER	DESCRIPTION	VALUE
N	Number of DPD beads	3000
$\bar{\Omega}$	Simulation box volume	$10 \times 10 \times 10$
\bar{r}_c	Cut-off radius	1.0
$\bar{\rho}$	Dimensionless density	3.0
n	Number density	3
$\frac{n_c}{k_B T}$	Dimensionless density ^a	12.57
$\bar{\sigma}$	Noise (random) parameter	3.0, 6.0, 8.0
$\bar{\gamma}$ ^b	Friction (dissipative) parameter	4.5, 18.0, 32.0
$\bar{\Lambda}$ ^c	Lambda parameter [33]	1.5, 6.0, 10.67
$\Delta\bar{t}$	Time step	0.005, 0.02, 0.04
λ	Factor for GW integrator	0.65
\bar{s}	Overlapping factor [33]	1.4422
v_T	Thermal velocity [33]	1

^a $n_c = \frac{4}{3} \pi \bar{r}_c^3$.

^bCalculated using the fluctuation-dissipation theorem [3,4].

^c $\bar{\Lambda}$ is the same as Ω in [33].

search [13]. Consequently, detailed theoretical analyses of the convergence and stability of typical DPD algorithms, which would enable much-needed improvements in accuracy, have not yet been reported. Despite this difficulty, several groups have made important contributions by proposing new integrators for DPD. There has also been previous work done to test and compare the properties of some of these integrators [14–16].

Originally, Eq. (1) was integrated using the simple Euler method [1] used mainly for deterministic ordinary differential equations. However, two temperature-related problems have been found with this integrator: (1) a discrepancy between the kinetic temperature calculated from particle velocities and the “set” temperature fixed in the system [1] and (2) variation in the kinetic temperature with integration algorithm and time step. Several investigators have proposed new integrators to address these issues. Groot and Warren [5] proposed a modified velocity Verlet method that changes the contribution of the velocity used to calculate the new dissipative forces. This method has been widely used and shows a relatively small change in kinetic temperature against the set temperature of the system. Pagonabarraga *et al.* [11] proposed the self-consistent scheme to make the maximum attainable time step independent of the algorithm. They used a variation in the traditional leap-frog algorithm used in molecular dynamics simulations and found that the drift in temperature and the spurious structure in the radial distribution function for two-dimensional (2D) systems were minimal. Besold *et al.* [14] and Vattulainen *et al.* [15] proposed variants of the self-consistent scheme and compared the temperature conservation, radial distribution function, and tracer diffusion coefficient of simple and ideal fluids for various integrators. The above integrators were all inspired by conventional schemes, such as those in molecular dynamics,

used to solve deterministic equations. The conventional schemes have been found to be better than the Euler scheme, but their theoretical behavior and order of convergence are still unclear [17]. Other schemes inspired by operator splitting techniques [18], Trotter expansions [19,20], alternative approaches [21,22], and multiple time step schemes [23] have also been reported and show significant improvements over previous methods.

Integrators for DPD have traditionally been evaluated based on temperature conservation and *static* properties such as radial distribution function. Evaluation against *dynamic* fluid transport properties provides another sensitive probe of the integration algorithm, but few such studies have been performed. Tracer diffusion coefficient calculations based on the Einstein expression have been reported [14,15] and non-equilibrium Lees-Edwards [11] and periodic Poiseuille flow [24] simulations have provided data on shear viscosity. Transport properties may also be calculated by Green-Kubo integration [25] of velocity and stress autocorrelation functions. Although widely used in molecular dynamics simulations [26–29], only two DPD studies [24,30] have applied the Green-Kubo approach for shear viscosity calculations. The investigations of Keaveny *et al.* [30] were limited to the Groot/Warren scheme with constant friction parameters. Backer *et al.* [24], however, studied the effect of friction, density, and temperature on the shear viscosity, but also only for the Groot/Warren integrator.

In this paper, we investigate the combined effects of integration scheme, time step, and friction parameter on the velocity and stress autocorrelation decay of a single component ideal DPD fluid. We also report the diffusion coefficient and shear viscosity calculated using Green-Kubo integrals. Dimensionless quantities are shown with an overbar [6] and the values are given in dimensionless DPD units ($\bar{m}=1.0$, $\bar{r}_c=1.0$, $k_B T=1.0$). The Groot/Warren [5] (GW), self-consistent [11] (SCPHF, named after the authors), self-consistent velocity Verlet [14,15] (SCVV), and the first and second order weak schemes developed by Shardlow [18] (S1 and S2) have been compared to check the effect of these algorithms on the dynamic properties of ideal fluids for three values of random noise parameter ($\bar{\sigma}=\{3.0, 6.0, 8.0\}$) and three values of time step ($\Delta\bar{t}=\{0.005, 0.02, 0.04\}$). Section II outlines the integration algorithms and discusses in detail the techniques used to implement them. Section III compares the performance of the integrators as a function of time step and random force parameter and discusses the results.

II. INTEGRATION ALGORITHMS

A. GROOT/WARREN INTEGRATOR

The Groot/Warren scheme is a multistep time integration technique based on a modified version of the Verlet [31] scheme used most often in molecular dynamics. This scheme is briefly discussed below. Velocities advanced by two fractions of a time step (λ and 0.5, respectively) are calculated

$$\bar{\mathbf{v}}_i(\bar{t} + \lambda \Delta\bar{t}) = \bar{\mathbf{v}}_i(\bar{t}) + \lambda \frac{\bar{\mathbf{F}}_i(\bar{t})}{m_i} \Delta\bar{t}, \quad (7)$$

$$\bar{\mathbf{v}}_i^o\left(\bar{t} + \frac{1}{2}\Delta\bar{t}\right) = \bar{\mathbf{v}}_i(\bar{t}) + \frac{1}{2}\frac{\bar{\mathbf{F}}_i(\bar{t})}{\bar{m}_i}\Delta\bar{t}. \quad (8)$$

Then, positions are advanced using the velocity at 0.5 time step velocity

$$\bar{\mathbf{r}}_i(\bar{t} + \Delta\bar{t}) = \bar{\mathbf{r}}_i(\bar{t}) + \bar{\mathbf{v}}_i^o\left(\bar{t} + \frac{1}{2}\Delta\bar{t}\right)\Delta\bar{t} \quad (9)$$

and forces are then advanced based on this new position and on the λ time step velocity

$$\bar{\mathbf{F}}_i(\bar{t} + \Delta\bar{t}) = \bar{\mathbf{F}}_i(\bar{\mathbf{r}}_i(\bar{t} + \Delta\bar{t}), \bar{\mathbf{v}}_i(\bar{t} + \lambda\Delta\bar{t})). \quad (10)$$

Finally, the velocity is advanced based on this new force and on the 0.5 time step velocity

$$\bar{\mathbf{v}}_i(\bar{t} + \Delta\bar{t}) = \bar{\mathbf{v}}_i^o\left(\bar{t} + \frac{1}{2}\Delta\bar{t}\right) + \frac{1}{2}\frac{\bar{\mathbf{F}}_i(\bar{t} + \Delta\bar{t})}{\bar{m}_i}\Delta\bar{t}. \quad (11)$$

The value of λ used in this paper is 0.65, which was first suggested by Groot/Warren for good numerical stability.

B. SELF-CONSISTENT INTEGRATOR

In the SCPHF scheme,

$$\bar{\mathbf{v}}_i\left(\bar{t} + \frac{1}{2}\Delta\bar{t}\right) = \bar{\mathbf{v}}_i\left(\bar{t} - \frac{1}{2}\Delta\bar{t}\right) + \frac{\bar{\mathbf{F}}_i(\bar{\mathbf{r}}_i(\bar{t}), \bar{\mathbf{v}}_i(t^*))}{\bar{m}_i}\Delta\bar{t}, \quad (12)$$

$$\bar{\mathbf{v}}_i(t^*) = \frac{1}{2}\left[\bar{\mathbf{v}}_i\left(\bar{t} - \frac{1}{2}\Delta\bar{t}\right) + \bar{\mathbf{v}}_i\left(\bar{t} + \frac{1}{2}\Delta\bar{t}\right)\right], \quad (13)$$

$$\bar{\mathbf{r}}_i(\bar{t} + \Delta\bar{t}) = \bar{\mathbf{r}}_i(\bar{t}) + \bar{\mathbf{v}}_i(t^*)\Delta\bar{t} + \frac{\bar{\mathbf{F}}_i(\bar{\mathbf{r}}_i(\bar{t}), \bar{\mathbf{v}}_i(t^*))}{2\bar{m}_i}[\Delta\bar{t}]^2 \quad (14)$$

forward half-step and backward half-step velocities are computed and their average is used to determine new positions $\bar{\mathbf{r}}_i(\bar{t} + \Delta\bar{t})$ and velocities $\bar{\mathbf{v}}_i(\bar{t} + \frac{1}{2}\Delta\bar{t})$. As the forward half-step velocity [Eq. (12)] depends on this average, iteration is required to obtain self-consistent velocities. Since the dissipative force is linear in velocity, Eq. (12) can be simplified further and an explicit update of velocities can be performed. Thus, both implicit and explicit solution methods may be applied in SCPHF. For clarity, we describe below the exact procedure used to implement the SCPHF integrator in this paper, as this has not been presented previously in the literature.

Converting Eqs. (12)–(14) to subscript notation simplifies the implementation of the SCPHF solution procedure. Here, the following mappings are used: $\mathbf{r}_i(t) \rightarrow \mathbf{r}_{i,n}$, $\mathbf{r}_i(t + \Delta t) \rightarrow \mathbf{r}_{i,n+1}$, $\mathbf{v}_i(t - \frac{1}{2}\Delta t) \rightarrow \mathbf{v}_{i,n}$, $\mathbf{v}_i(t + \frac{1}{2}\Delta t) \rightarrow \mathbf{v}_{i,n+1}$, and $\mathbf{F}_i(t) \rightarrow \mathbf{F}_{i,n}$, $\mathbf{F}_i(t + \Delta t) \rightarrow \mathbf{F}_{i,n+1}$. At each calculation step n in the implementation, all quantities are advanced a full time step. With the above mappings, Eq. (12) can be rewritten as

$$\bar{\mathbf{v}}_{i,n+1} = \bar{\mathbf{v}}_{i,n} + \frac{\Delta\bar{t}}{\bar{m}_i}\left\{\bar{\mathbf{F}}^C(\bar{\mathbf{r}}_{i,n}) + \bar{\mathbf{F}}^R(\bar{\mathbf{r}}_{i,n}) - \sum_{j \neq i} \bar{\gamma}_{ij}\bar{w}^D(\bar{\mathbf{r}}_{ij,n})\right. \\ \left. \times \left[\frac{1}{2}[\bar{\mathbf{v}}_{ij,n} + \bar{\mathbf{v}}_{ij,n+1}] \cdot \hat{\mathbf{r}}_{ij,n}\right] \hat{\mathbf{r}}_{ij,n}\right\}. \quad (15)$$

Since the dissipative force is linear in velocity, the terms can be separated into

$$\bar{\mathbf{v}}_{i,n+1} + \frac{1}{2}\frac{\Delta\bar{t}}{\bar{m}_i}\sum_{j \neq i} \bar{\gamma}_{ij}\bar{w}^D(\bar{\mathbf{r}}_{ij,n})[\bar{\mathbf{v}}_{ij,n+1} \cdot \hat{\mathbf{r}}_{ij,n}]\hat{\mathbf{r}}_{ij,n} \\ = \bar{\mathbf{v}}_{i,n} + \frac{\Delta\bar{t}}{\bar{m}_i}\left\{\bar{\mathbf{F}}^C(\bar{\mathbf{r}}_{i,n}) + \bar{\mathbf{F}}^R(\bar{\mathbf{r}}_{i,n}) - \frac{1}{2}\sum_{j \neq i} \bar{\gamma}_{ij}\bar{w}^D(\bar{\mathbf{r}}_{ij,n})\right. \\ \left. \times [\bar{\mathbf{v}}_{ij,n} \cdot \hat{\mathbf{r}}_{ij,n}]\hat{\mathbf{r}}_{ij,n}\right\}. \quad (16)$$

Equation (16) is slightly complicated as the new velocities of particle i depend on all the velocity components of particle j

$$[\bar{\mathbf{v}}_{ij,n+1} \cdot \hat{\mathbf{r}}_{ij,n}]\hat{\mathbf{r}}_{ij,n} = \frac{[\bar{\mathbf{r}}_{i,n} - \bar{\mathbf{r}}_{j,n}]}{|\bar{\mathbf{r}}_{ij}|}\left\{[\bar{v}_{ix,n+1} - \bar{v}_{jx,n+1}]\frac{[\bar{r}_{ix,n} - \bar{r}_{jx,n}]}{|\bar{\mathbf{r}}_{ij}|}\right. \\ + [\bar{v}_{iy,n+1} - \bar{v}_{jy,n+1}]\frac{[\bar{r}_{iy,n} - \bar{r}_{jy,n}]}{|\bar{\mathbf{r}}_{ij}|} \\ \left. + [\bar{v}_{iz,n+1} - \bar{v}_{jz,n+1}]\frac{[\bar{r}_{iz,n} - \bar{r}_{jz,n}]}{|\bar{\mathbf{r}}_{ij}|}\right\}. \quad (17)$$

Hence, Eq. (17) can be written as

$$M \cdot \bar{\mathbf{v}}_{i,n+1} = \bar{\mathbf{v}}_{i,n} + \frac{\Delta\bar{t}}{\bar{m}_i}\left\{\bar{\mathbf{F}}^C(\bar{\mathbf{r}}_{i,n}) + \bar{\mathbf{F}}^R(\bar{\mathbf{r}}_{i,n}) + \frac{1}{2}\bar{\mathbf{F}}^D(\bar{\mathbf{r}}_{i,n}, \bar{\mathbf{v}}_{i,n})\right\}, \quad (18)$$

where M is a matrix whose entries correspond to the left hand side of Eq. (16). As the interactions between particles are pairwise and symmetric, the matrix M is symmetric and positive definite (SPD).

There are two ways to solve the above system of equations—one involves inverting the matrix and the second involves solving the equations using an iterative solver. For the second, we use the Conjugate Gradient (CG) solver implemented in the widely used parallel PETSC package [32]. CG is particularly suited for SPD systems and has faster convergence than other iterative schemes. For direct inversion, we use the lower triangular upper triangular (LU) decomposition technique in PETSC. Note however that using LU or other direct techniques to solve the vector Eq. (18) can be computationally very expensive as it involves explicitly forming the matrix entries. For all our SCPHF calculations, we have used a relative tolerance in the solver of 10^{-14} .

C. SELF-CONSISTENT VELOCITY VERLET INTEGRATOR

The SCVV scheme is a variant of the velocity Verlet scheme that enforces self-consistency between set and kinetic temperatures at a single time step by functional itera-

tion of the velocities using the dissipative forces at the end of the Verlet steps [Eqs. (7)–(11)]. Positions are not updated in the iteration and the same value calculated at the end of the step in Eq. (11) is used for all iteration steps.

At the j^{th} iteration step, the dissipative forces are calculated using the positions and the $[j-1]^{\text{th}}$ iteration step velocities

$$\bar{\mathbf{F}}_i^D(j) = \bar{\mathbf{F}}_i^D(\bar{\mathbf{r}}_i, \bar{\mathbf{v}}_i(j-1)). \quad (19)$$

The new velocities in the iteration are updated using

$$\bar{\mathbf{v}}_i(j) = \bar{\mathbf{v}}_i(j-1) + \frac{\Delta\bar{t}}{2}\bar{\mathbf{F}}_i^D(j). \quad (20)$$

The velocity at iteration $j=0$ corresponds to that found in Eq. (11). The new kinetic temperature of the system is calculated as an average over all particles i in the system

$$\frac{\bar{m}_i[\bar{\mathbf{v}}_i(j)]^2}{k_B T} = \frac{\sum_i \bar{m}_i[\bar{\mathbf{v}}_i(j)]^2}{3[N-1]}. \quad (21)$$

If the kinetic temperature in Eq. (21) differs from the set temperature, the process in Eqs. (19)–(21) is repeated until a specified tolerance is reached. In the present paper, a tolerance of 10^{-3} is used. The self-consistent velocity and force calculated at the end of the iteration procedure are input to the calculations at the next time step [Eqs. (7)–(11)].

D. SHARDLOW FIRST ORDER INTEGRATOR (S1)

The Shardlow ‘‘S1’’ integrator is a first order weakly convergent scheme based on splitting the force field into a sum of conservative and dissipation-random terms [18]. The conservative system is solved using the regular velocity Verlet method whereas the dissipative and random forces are solved implicitly in a manner that conserves linear momentum in the process. The first order splitting leads to the following algorithm for particle pairs i, j :

$$\begin{aligned} \bar{\mathbf{v}}_{i,n+1/2} = & \bar{\mathbf{v}}_{i,n} - \frac{1}{2\bar{m}}\bar{\gamma}_{ij}[\bar{w}_{ij}^D(\bar{\mathbf{r}}_{ij,n})][\bar{\mathbf{v}}_{ij,n} \cdot \hat{\mathbf{r}}_{ij,n}]\hat{\mathbf{r}}_{ij,n}d\bar{t} \\ & + \frac{1}{2\bar{m}}\sqrt{2\bar{\gamma}_{ij}k_B T}[\bar{w}_{ij}^R(\bar{\mathbf{r}}_{ij,n})]\psi_{ij}\hat{\mathbf{r}}_{ij,n}d\bar{t}^{1/2}, \end{aligned} \quad (22)$$

$$\begin{aligned} \bar{\mathbf{v}}_{j,n+1/2} = & \bar{\mathbf{v}}_{j,n} + \frac{1}{2\bar{m}}\bar{\gamma}_{ij}[\bar{w}_{ij}^D(\bar{\mathbf{r}}_{ij,n})][\bar{\mathbf{v}}_{ij,n} \cdot \hat{\mathbf{r}}_{ij,n}]\hat{\mathbf{r}}_{ij,n}d\bar{t} \\ & - \frac{1}{2\bar{m}}\sqrt{2\bar{\gamma}_{ij}k_B T}[\bar{w}_{ij}^R(\bar{\mathbf{r}}_{ij,n})]\psi_{ij}\hat{\mathbf{r}}_{ij,n}d\bar{t}^{1/2}, \end{aligned} \quad (23)$$

$$\begin{aligned} \bar{\mathbf{v}}_{i,n+1} = & \bar{\mathbf{v}}_{i,n+1/2} + \frac{1}{2\bar{m}}\sqrt{2\bar{\gamma}_{ij}k_B T}[\bar{w}_{ij}^R(\bar{\mathbf{r}}_{ij,n})]\psi_{ij}\hat{\mathbf{r}}_{ij,n}d\bar{t}^{1/2} \\ & - \frac{1}{2\bar{m}}\frac{\bar{\gamma}_{ij}[\bar{w}_{ij}^D(\bar{\mathbf{r}}_{ij,n})]d\bar{t}}{1 + \bar{\gamma}_{ij}[\bar{w}_{ij}^D(\bar{\mathbf{r}}_{ij,n})]d\bar{t}}\{[\bar{\mathbf{v}}_{ij,n+1/2} \cdot \hat{\mathbf{r}}_{ij,n}]\hat{\mathbf{r}}_{ij,n} \\ & + \sqrt{2\bar{\gamma}_{ij}k_B T}[\bar{w}_{ij}^R(\bar{\mathbf{r}}_{ij,n})]\psi_{ij}\hat{\mathbf{r}}_{ij,n}d\bar{t}^{1/2}\}, \end{aligned} \quad (24)$$

$$\begin{aligned} \bar{\mathbf{v}}_{j,n+1} = & \bar{\mathbf{v}}_{j,n+1/2} - \frac{1}{2\bar{m}}\sqrt{2\bar{\gamma}_{ij}k_B T}[\bar{w}_{ij}^R(\bar{\mathbf{r}}_{ij,n})]\psi_{ij}\hat{\mathbf{r}}_{ij,n}d\bar{t}^{1/2} \\ & + \frac{1}{2\bar{m}}\frac{\bar{\gamma}_{ij}[\bar{w}_{ij}^D(\bar{\mathbf{r}}_{ij,n})]d\bar{t}}{1 + \bar{\gamma}_{ij}[\bar{w}_{ij}^D(\bar{\mathbf{r}}_{ij,n})]d\bar{t}}\{[\bar{\mathbf{v}}_{ij,n+1/2} \cdot \hat{\mathbf{r}}_{ij,n}]\hat{\mathbf{r}}_{ij,n} \\ & + \sqrt{2\bar{\gamma}_{ij}k_B T}[\bar{w}_{ij}^R(\bar{\mathbf{r}}_{ij,n})]\psi_{ij}\hat{\mathbf{r}}_{ij,n}d\bar{t}^{1/2}\}. \end{aligned} \quad (25)$$

The next step involves updating the velocities based on the conservative forces using the regular Verlet algorithm [31].

E. SHARDLOW SECOND ORDER INTEGRATOR (S2)

The weakly converging second order scheme ‘‘S2’’ is similar to the S1 scheme where Eqs. (22)–(25) are solved initially using a time step of $d\bar{t}/2$ instead of $d\bar{t}$ that is used in S1. This is followed by updating the positions and velocities based on the conservative forces using the Verlet algorithm. Finally, Eqs. (22)–(25) are used again to update the new positions and velocities with a time step of $d\bar{t}/2$.

III. RESULTS AND DISCUSSION

A. TEMPERATURE CONSERVATION AND RADIAL DISTRIBUTION FUNCTION

We have independently tested the GW and SCVV integrators for their temperature conservation properties and radial distribution function for the parameters listed in Table I. The integrators show good temperature control up to a time step of 0.04 and noise parameters of 3 and 6, which compares very well with the investigations of other groups [5,14,15]. The GW integrator starts to deviate at a noise parameter of 8 and time step of 0.04, as expected [5]. The radial distribution function behaves well at short time steps but shows pronounced structure at large time steps, which has also been reported previously. The performance of the SCPHF integrator has been investigated by only one group [11] for a 2D ideal system. We performed our own test of this integrator for a three-dimensional (3D) system with the parameters given in Table I, and using the explicit implementation described in Sec. II. The results are not shown here for brevity. The total simulation time for this system was 200 000 time steps and time averaging was performed over the last 150 000 time steps. The SCPHF integrator shows very good temperature control for the time steps and noise parameters used. The error is computed as the standard deviation of the mean and is 1–2 % of the set temperature. The radial distribution function is in good agreement with the theoretical value of one. The present temperature conservation and radial distribution function results are in agreement with the previous 2D results reported in the literature [11]. The S1 and S2 integrators were also tested on the same system and outperformed the other integrators in terms of temperature control. The error in the set temperature was found to be less than 1%. The exceptionally good temperature control of the Shardlow integrators has been reported in independent tests by Shardlow [18] and Nikunen *et al.* [16] and is in agreement with our tests.

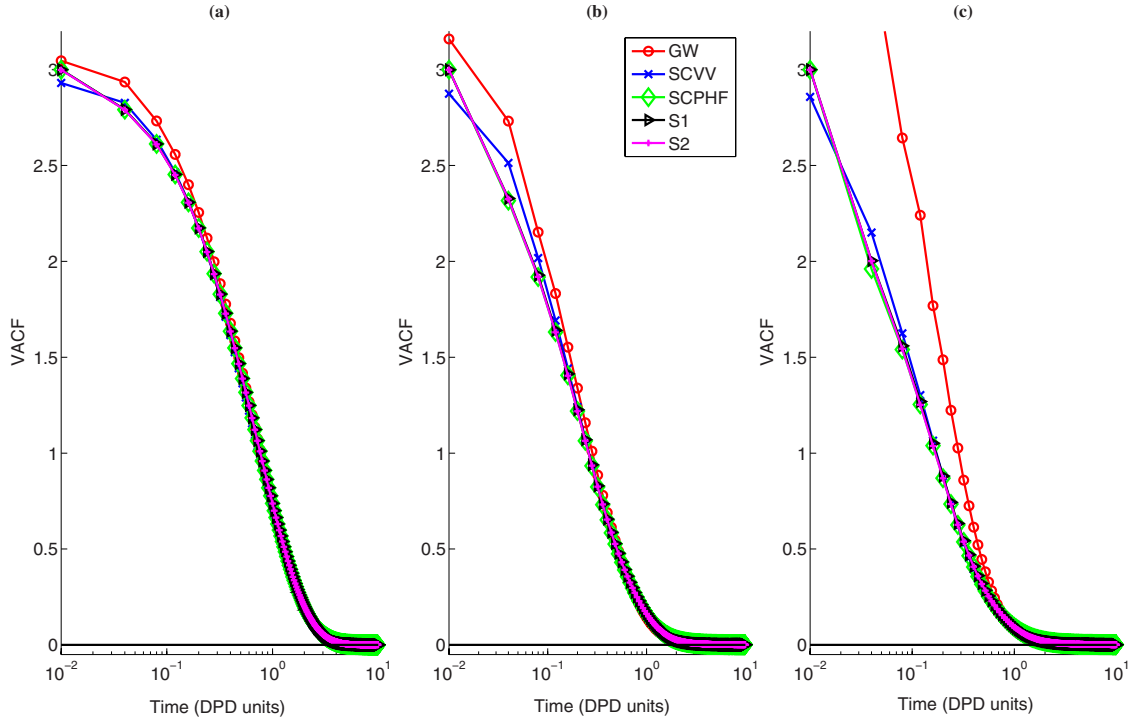


FIG. 1. (Color online) Comparison of VACF for all integrators at $\Delta t=0.04$ and at different values of $\bar{\Lambda}$; (a) $\bar{\Lambda}=1.5$, (b) $\bar{\Lambda}=6.0$, and (c) $\bar{\Lambda}=10.67$; the solid lines are fit to the simulation results (symbols).

B. COMPUTATIONAL EFFICIENCY

The computational efficiency of the various integrators was tested for the system with parameters given in Table I at the noise parameter value of 3.0 and time step of 0.04. The test case was run on a dual-core Pentium 3 GHz Xeon 5160 system with 8 GB RAM. The time taken per time step was recorded for 1000 time steps and averaged over the last 500 time steps. The time taken to calculate the Verlet list was calculated separately and removed from the total time to just get the information regarding the integration process. The GW scheme was found to be the fastest of all the integrators. This has also been confirmed by other studies and has been one of the main reasons for its popularity as an integration scheme. The SCVV scheme is approximately 1.6 times slower than GW followed by the S1 scheme that is 1.9 times slower. Shardlow's S2 scheme is almost 2.8 times slower than GW. The slowest scheme is SCPHF, which is 5.1 times slower than GW and almost 3 times slower than SCVV and S1. Clearly, GW stands out as the fastest and SCPHF as the most computationally expensive scheme of the integrators studied here.

C. VELOCITY AUTOCORRELATION FUNCTION

Español and Serrano [33] have shown using mode-coupling theory that the velocity autocorrelation function (VACF) decays exponentially at low dimensionless friction parameter $\bar{\Lambda} = \frac{\gamma \tau_c}{d \bar{v}_T}$ and low overlapping factor $\bar{s} = \frac{\bar{r}_c}{n^{-1/d}}$. Here, d is the dimensionality of the system and \bar{v}_T is the thermal velocity of the bead ($\sqrt{k_B T / m}$). They also calculated VACF using 2D DPD simulations in which they varied

the friction $\bar{\Lambda}$ and kept the box size and overlapping factor constant. Here, we report the first calculation of VACF for a 3D system using various integrators, time steps, and friction values. To facilitate comparison with the results of Español and Serrano, we have chosen to compare the decay using the parameter $\bar{\Lambda}$ and keeping the overlapping factor constant at $\bar{s}=1.4422$.

The VACF is calculated from velocity data saved at each time step. Since the 3D DPD system for the parameters in Table I has a low Schmidt number [$\sim O(1)$] [5], the DPD beads diffuse as quickly as the momentum flux relaxes. This large diffusion coefficient necessitates calculation of the VACF at every time step, as opposed to every fifth or 10th time step as is often done in molecular dynamics simulations, to best capture rapidly changing velocity variations. The time origins were spaced at a value of 0.04, which is also the largest time step used in the simulations. We calculate the correlation function for all beads in the system and average over these at each time origin, as this has been shown to improve the statistics. Here, the error bar represents the standard error of the mean (standard deviation divided by the square root of the product of number of time steps and number of beads in the system). This value was found to be approximately 10^{-6} .

Figure 1 compares the decay of GW, SCPHF, SCVV, S1, and S2 integrators at a time step of 0.04 and at different values of $\bar{\Lambda}$. At zero time, the VACF should have a value of $\langle \bar{v}(0)^2 \rangle = 3k_B T$, which comes from equipartition and is used to define the kinetic temperature. For $k_B T = 1.0$, this translates to a value of three at zero time. The GW and SCVV integrators show differences in the zero time VACF value when

TABLE II. Diffusion coefficient values for all the integrators at a time step of 0.04. The quantities in parentheses are uncertainty $\times 10^4$. Uncertainty is calculated as the standard deviation averaged over the first 30 DPD time units.

	GW	SCVV	SCPHF	S1	S2	THEORY
$\bar{\Lambda}=1.5$						
MSD	0.7116	0.6856	0.7340	0.7212	0.6972	0.67 [4]
VACF	0.7172 (7.24)	0.6915 (2.59)	0.7103 (3.36)	0.7120 (6.75)	0.7113 (5.98)	0.531[5]
$\bar{\Lambda}=6.0$						
MSD	0.3048	0.2944	0.2848	0.2820	0.2913	0.167[4]
VACF	0.3027 (6.60)	0.2898 (8.38)	0.2879 (8.28)	0.2894 (9.96)	0.2885 (8.71)	0.133[5]
$\bar{\Lambda}=10.67$						
MSD	0.3182	0.2123	0.2105	0.2138	0.2097	0.094[4]
VACF	0.3175 (6.24)	0.2098 (9.43)	0.2083 (10.3)	0.2101 (8.92)	0.2087 (9.88)	0.075[5]

compared to the SCPHF, S1, and S2 integrators. The SCPHF, S1, and S2 integrators are very good in maintaining the temperature of the system, which is evidenced by the good match with the value of three at zero time, for all $\bar{\Lambda}$ values. The GW integrator diverges at a time step of 0.04 at $\bar{\Lambda}=10.67$, which is clearly shown by the large deviation in the VACF profile in Fig. 1. All the integrators show similar decay behavior at smaller time steps of 0.005 and 0.02 for all values of $\bar{\Lambda}$ (not shown for brevity). It is also interesting to note that the SCPHF, S1, and S2 integrators show almost identical decay profiles for all $\bar{\Lambda}$ values. Since these algorithms are based on implicit definitions of the dissipative forces, the decay profiles look almost indistinguishable.

The VACF (normalized to its initial values) was also checked for the exponential decay at different $\bar{\Lambda}$ values. For very small values of friction, mode-coupling theory predicts exponential decay of the VACF [33]. The DPD results for the smallest $\bar{\Lambda}$ value closely follow the exponential behavior at all times. As $\bar{\Lambda}$ increases, both exponential and simulation results decay more rapidly. Also, deviation of the simulation results from exponential behavior becomes evident at higher $\bar{\Lambda}$ and is more pronounced as $\bar{\Lambda}$ increases. This deviation arises from collective behavior of the DPD beads, which leads to considerably slower decay than exponential. At long times, both exponential and simulation results converge to zero. The above 3D trends are qualitatively similar to those observed by Español and Serrano in the 2D studies and serve as a good validation of the Español theory for VACF decay. The more rapid long time VACF decay as $\bar{\Lambda}$ increases is reasonable since the diffusion coefficient is expected to decrease as $\bar{\Lambda}$ increases. Further discussion of the relation between VACF and diffusion coefficient is given in the next section.

The decay profiles with changes in integrator at different time steps only show deviations at $\bar{\Lambda}=10.67$ for the GW

integrator at the highest time step. All the other integrators show little or no variation with time step.

D. DIFFUSION COEFFICIENT

Although previous calculations of the diffusion coefficient have been performed [5,14,15], they have been limited to low friction values and a few integrators using the mean square displacement (MSD) approach.

$$\bar{D} = \lim_{\bar{t} \rightarrow \infty} \frac{1}{3\bar{t}} \langle |\bar{\mathbf{r}}(\bar{t}) - \bar{\mathbf{r}}(0)|^2 \rangle. \quad (26)$$

Here, we address these issues by reporting the first 3D Green-Kubo calculation of diffusion coefficient. We also report MSD calculations of diffusion coefficient at various time steps and friction parameters for validation.

The diffusion coefficient \bar{D} is calculated using both MSD approach and Green-Kubo integration of the VACF [25]

$$\bar{D} = \frac{1}{3} \int_0^\infty dt \langle \bar{\mathbf{v}}_i(\bar{t}) \cdot \bar{\mathbf{v}}_i(0) \rangle. \quad (27)$$

The diffusion coefficient data for the three integrators at different friction values and at the largest time step of 0.04 are presented in Table II. The largest time step serves as the most rigorous test of the integration schemes. Also, theoretical diffusion coefficient values were calculated from mean-field theory expressions [5] and from expressions [4] derived for the low friction limit using the Fokker-Planck-Boltzmann (FPB) equation for DPD and are also listed in the table. Specific details of the calculations involving Eq. (27) are described in the Appendix.

For all cases, the diffusion coefficient values decrease with increasing friction. This is an expected trend since diffusion is hindered at higher friction and the area under the VACF curve decreases. At low friction, the diffusion coeffi-

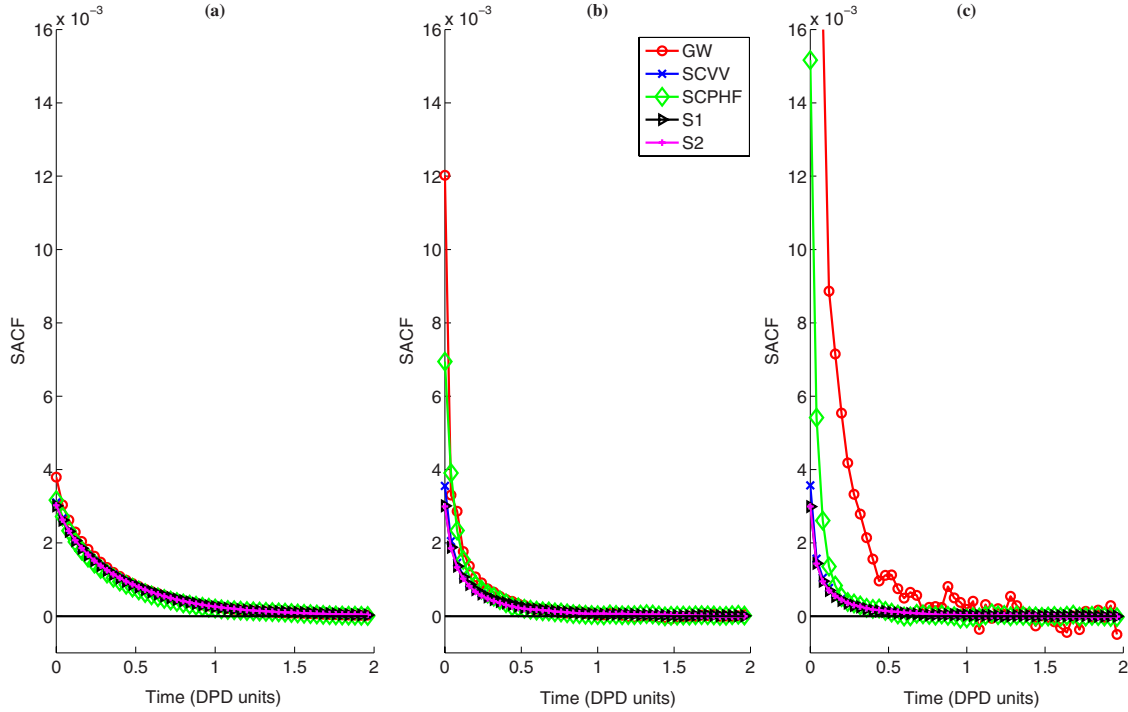


FIG. 2. (Color online) Comparison of SACF for all integrators at $\Delta\bar{t}=0.04$ and at different values of $\bar{\Lambda}$; (a) $\bar{\Lambda}=1.5$, (b) $\bar{\Lambda}=6.0$, and (c) $\bar{\Lambda}=10.67$; the solid lines are to fit the simulation results (symbols).

coefficients are 30–35 % higher than the theoretical predictions from Groot/Warren [5]. This is consistent with results reported for tracer diffusion coefficients [15] where the variation from theory is roughly 33%. In contrast, the values differ from the Marsh theory [4] by only 5–6 %. Hence, the Marsh theory predictions appear to be more accurate than the Groot/Warren theory. This is to be expected since the Marsh theory derives the results using the FPB equation, which is more accurate at low density, low friction limits. At higher friction values, the collective behavior is dominant and the kinetic theory results do not give correct predictions for transport coefficients, as the theoretical results were only derived for a low friction, low density limit. However, we list the values obtained at high friction in Table II to get an estimate of the deviation.

The MSD results and the Green-Kubo calculations show excellent agreement within statistical error for all cases except the GW, $\bar{\Lambda}=10.67$ case where the integration algorithm fails and shows a higher than usual set temperature (and hence a larger diffusion coefficient). Although theoretical results are not available for higher friction limits, the good agreement between MSD and Green-Kubo calculations (as is the case in the low friction limit) supports the correctness of the values. The integrators were run at different (lower than 0.04) time steps (not shown) to see the effects on the results. The VACF data exhibited minor differences in the decay profiles of the different integrators with change in time steps and hence the same minor differences were observed in the diffusion coefficients as a function of time step.

E. STRESS AUTOCORRELATION FUNCTION

Few calculations of the stress autocorrelation function (SACF) for DPD systems have been performed in the litera-

ture [24,30], and none of these studies provide temporal plots of SACF. Here, we investigate SACF and its dependence on integrator, friction, and time step. The stress calculations for the entire system were carried out using the Irving-Kirkwood stress tensor [34]

$$\bar{\Gamma}_{pq} = -\frac{1}{\bar{\Omega}} \left\{ \sum_i \bar{m}_i [\bar{v}_{i,p} \bar{v}_{i,q}] + \frac{1}{2} \sum_i \sum_{j \neq i} \bar{r}_{ij,p} \bar{F}_{ij,q}^D \right\}, \quad (28)$$

where $\bar{\Gamma}_{pq}$ is the pq^{th} entry of the stress tensor matrix. The SACF was calculated using the expression $\langle \bar{\Gamma}_{pq}(\bar{t}) \bar{\Gamma}_{pq}(0) \rangle$. To validate the stress autocorrelation calculations, we computed the value of the correlation $\langle \bar{\Gamma}_{xx}(0) \bar{\Gamma}_{xx}(0) \rangle_t$. At low friction, the kinetic stress terms are more dominant than the dissipative terms. The $\bar{\Gamma}_{xx}$ term is one part of the pressure tensor and from equipartition $\bar{\rho} \bar{k}_B \bar{T} \approx 3.0$ [5], so the value of $\langle \bar{\Gamma}_{xx}(0) \bar{\Gamma}_{xx}(0) \rangle_t$ should be around 9.0. We observe this value in our simulations. Only the dissipative force appears in Eq. (28), as the random forces do not contribute to the calculation of instantaneous transport coefficients [35,36]. Since the fluid is ideal, the conservative force contribution is exactly zero. The SACF plots are shown in Fig. 2 for the xy component of the stress tensor. Recently, some questions have been raised with regard to the validity of Green-Kubo relations for calculating transport coefficients using stochastic equations such as DPD, and alternate expressions have been proposed [35,37]. However, in this context there still seem to be some controversial issues, which may warrant further investigation but are beyond the scope of this paper.

Comparison of the integrators at various friction values reveals several trends. The results are plotted at a time step

TABLE III. Shear viscosity values for all the integrators at a time step of 0.04. The quantities in parentheses are uncertainty $\times 10^1$. Uncertainty is calculated as the standard deviation averaged over the first 100 DPD time units.

	GW	SCVV	SCPHF	S1	S2	THEORY/PREVIOUS WORK
$\bar{\Lambda}=1.5$						
SACF	1.1328 (1.47)	1.0309 (1.28)	0.8448 (1.73)	1.1988 (1.37)	1.2493 (1.39)	1.045 [4] 0.957 [5]
NEDPD	1.3242 (7)	1.0823 (5.56)	1.2675 (5.72)	1.1129 (5.54)	1.0688 (5.53)	1.5 [24]
$\bar{\Lambda}=6.0$						
SACF	0.8055 (0.89)	0.5396 (0.73)	0.5654 (1)	0.4828 (0.50)	0.5328 (0.64)	0.43 [4] 0.845 [5]
NEDPD	1.0425 (11.5)	0.5402 (6.01)	0.9600 (8.29)	0.5342 (5.58)	0.4605 (5.58)	3.2 [24]
$\bar{\Lambda}=10.67$						
SACF	4.0808 (7.53)	0.4120 (0.55)	0.7101 (1)	0.3178 (0.37)	0.3008 (0.49)	0.461 [4] 1.261 [5]
NEDPD	1.4232 (25.7)	0.4070 (6.08)	1.0365 (12.3)	0.4045 (5.59)	0.3383 (5.60)	

of 0.04 in Fig. 2. In this figure, all integrators show faster SACF decay with increasing friction. The higher friction results in higher dissipation and hence a faster decorrelation of shear stresses in the system. All integrators have the same zero time stress autocorrelation value (approximately 3×10^{-3}) at low friction ($\bar{\Lambda}=1.5$). As friction increases, the GW and SCPHF integrators show increased zero time stress autocorrelation values while the value for the S1 and S2 integrators remains at 3×10^{-3} . The SCVV integrator shows slight increase in the zero time values as friction increases. At low friction, the effect of the dissipative contribution to stress is negligible and hence the SCVV integrator behaves in an identical fashion as the GW or SCPHF integrator. However, as the friction increases in the system, the SCVV algorithm takes more iterations to stabilize the temperature by constantly iterating on the dissipative term. The S1 and S2 integrators follow the decay of the SCVV algorithm closely beyond the zero stress value. The operator splitting in the S1 and S2 integrators also focuses on the dissipative and random terms particularly as shown in Eqs. (22)–(25). This could one of the reasons why the S1, S2, and SCVV algorithms show similar decay profiles.

The effect of time step on SACF for all the integrators at the low and high friction limits is also investigated (not shown). Invariance with time step is typically viewed as a good integrator characteristic and all integrators perform very well at low friction by showing almost identical decay profiles.

F. SHEAR VISCOSITY

Numerous theoretical and DPD studies of dynamic shear viscosity have been performed in the literature. Theoretical

work includes studies based on the Fokker-Planck-Boltzmann equation [4], mean-field theory [5], Mori theory of projection operators [38], and Boltzmann pair collision theory [39]. Numerical studies for ideal fluids have applied the Lees-Edwards shear flow method [11,24,30], the periodic Poiseuille flow method [24], and Green-Kubo integration of the SACF autocorrelation [24,30]. The numerical studies have all been done on disparate systems and hence it is difficult to compare the shear viscosity values. Also there have been no previous studies on the SCVV integrator and only 2D studies using the SCPHF integrator. Here, we report the first detailed parametric study between the integrators for three different friction values, which span the range of the previous studies that have used the GW integrator primarily. We also present a detailed comparison with theoretical predictions, nonequilibrium DPD (NEDPD) and other studies wherever possible to present a complete picture of the shear viscosity trends of an ideal DPD fluid.

The shear viscosity calculations for the different cases studied in this paper are shown in Table III. The table also shows our calculations based on theoretical predictions of Marsh *et al.* [4], Groot/Warren [5] and data from simulations of Backer *et al.* [24] (taken from the figures wherever possible) for comparison. The NEDPD calculations are also presented in Table III and were done by subjecting the system to a boundary-driven Couette flow. Details of the simulation are given below.

The shear viscosity calculations were done for the GW integrator and for the newer SCPHF, SCVV, S1, and S2 integrators as a function of time step and friction. The dynamic shear viscosity for the pq component of the stress tensor is given by the Green-Kubo relation [25]

$$\bar{\eta}_{pq} = \frac{\bar{\Omega}}{k_B T} \int_0^\infty d\bar{t} \langle \bar{\Gamma}_{pq}(\bar{t}) \bar{\Gamma}_{pq}(0) \rangle. \quad (29)$$

Since the system is homogeneous and isotropic, averages over the xy , yz , and zx components were taken for better statistics. To compute the shear viscosity, it is required to calculate the area under the autocorrelation profiles. In the present work, the SACF was found to fluctuate more rapidly than the VACF. At long times, the mean of these fluctuations was close to zero (10^{-6}), so it was assumed that the particular choice of “cut-off” point used as the upper time limit in the integral would not dramatically affect the results. In this study, we have chosen 100 DPD units as the upper time limit for all cases. Further details of the actual calculations for shear viscosity may be found in the Appendix.

In the nonequilibrium case, the shear flow was generated using a boundary-driven method. The walls were subjected to an external velocity of 0.5 DPD units and the bounce-forward [40] boundary condition was used at the walls to ensure the correct velocity profile. Since DPD provides a natural thermostat to the underlying system, no additional temperature control was enforced. The stresses were calculated using Eq. (28) and the shear viscosity was calculated using the following expression [36]:

$$\bar{\eta}_{xy} = \frac{\langle \bar{\Gamma}_{xy} \rangle}{\dot{\gamma}}. \quad (30)$$

The average $\langle \dots \rangle$ in Eq. (30) was calculated over 100 000 time steps after a linear velocity profile that matched the imposed velocity at the boundaries was observed. The error in the viscosity was calculated as the standard deviation and is reported in Table III for all the cases.

The shear viscosity for the DPD system is the sum of kinetic and dynamic contributions [4]. The kinetic contribution arises from the diffusion of beads and the dynamic contribution arises from the resistance of motion between layers of DPD beads. The kinetic contribution decreases and the dynamic contribution increases with increase in friction in the system. Hence, at very low friction, the kinetic contribution is dominant and at higher values of friction, the dynamic contribution is dominant. Even though both theories [4,5] predict this behavior, the rates at which the decrease/increase with friction happens is very different as predicted by the equations. Both theories show similar decrease at low values of $\bar{\Lambda}$ as shown in Fig. 3. At higher values of $\bar{\Lambda}$, the GW theory shows a sharp increase in the viscosity, whereas the curve from the Marsh theory only increases gradually. These differences account for the different predictions by the two theories shown in Table III.

Unlike velocity, $\bar{\Gamma}$ is a property of the whole system and cannot be averaged over all beads in the system. For this reason, the statistical errors in transport properties calculated from the SACF (shear viscosity) are generally higher than those calculated from the VACF (diffusion coefficient) [41]. This has been observed previously in DPD systems by Backer *et al.* [24], and is borne out by our own studies of shear viscosity.

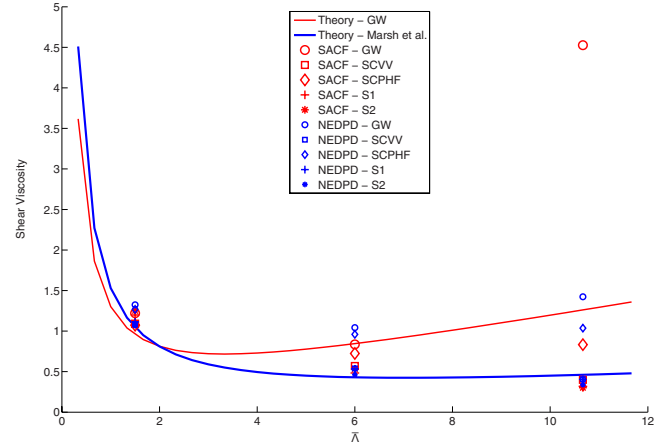


FIG. 3. (Color online) Shear viscosity comparisons between theory, SACF, and NEDPD calculations at $\Delta\bar{t}=0.04$.

The shear viscosity data from Table III are plotted in Fig. 3, without the error bars to avoid cluttering the graph. All viscosity values but one lie between or near the theoretical predictions. The only outlier point in Table III and Fig. 3 is the GW integrator at a time step of 0.04, $\bar{\Lambda}=10.67$. At low values of $\bar{\Lambda}$, all the data points sit on the lines that represent the theoretical predictions to within statistical limits. This is a good validation for using either of the GW and Marsh theories for shear viscosity calculations unlike the diffusion coefficient where the GW theory was off by 33%.

With increase in friction, Backer *et al.* [24] report a consistent increase in shear viscosity as shown in their calculations and in Table III. This is not observed in the present results and increase in viscosity with friction is only valid at very high friction values. As the friction is increased, the shear viscosity values fall in between the two theoretical curves. Even though the theoretical predictions have been derived for a low friction, low density limit, they seem to hold very well in the high friction, low density limit. The high friction, high density limit was not tested here and is expected to give significant deviations from the values shown in Fig. 3.

There are no significant deviations of the shear viscosity data with time steps, which is expected as the transport properties must be independent of the time step. The outlier point for the GW integrator at $\bar{\Lambda}=10.67$ and $\Delta\bar{t}=0.04$ occurs because of the failure of the algorithm at high friction and large time steps. Comparing the integrators shows that the shear viscosities calculated using the SCVV, S1, and S2 algorithms either lie close to the lower curve (Marsh *et al.*) or below it at high $\bar{\Lambda}$, thus underpredicting the values. The S1 and S2 integrators values are lower than the Marsh predictions by at least 27%. At low $\bar{\Lambda}$, the viscosities calculated by all the integrators fall close to the theoretical predictions. The SCPHF integrator has no outlier points and all the values lie within or close to the theoretical curves.

Figure 3 also shows no significant deviations between the SACF and NEDPD results, which is to be expected because of linear response. However, the error calculations reported in Table III are significantly higher for the NEDPD results

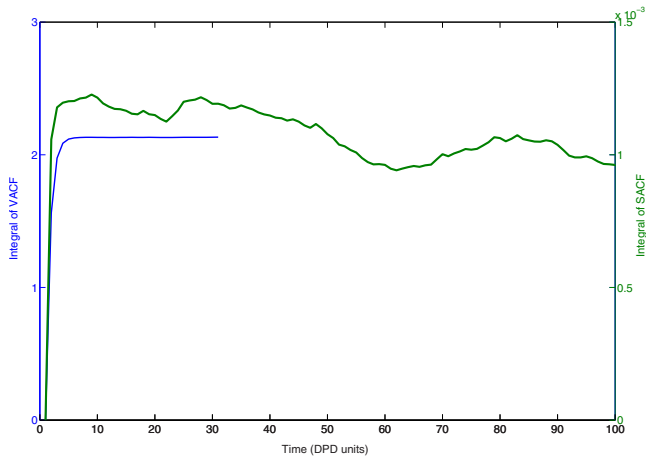


FIG. 4. (Color online) Integral of VACF (smooth line) calculated for 30 time units at intervals of 1 unit and integral of SACF (jagged line) calculated for 100 time units at intervals of 1 unit for the SCPHF integrator at $\bar{\Lambda}=1.5$; $\Delta\bar{t}=0.04$.

than the SACF calculations, especially at higher friction values. This was found mainly in the GW and the SCPHF integrators as shown in Table III. As the system is being driven away from equilibrium while shearing, the stress fluctuations are higher and the DPD thermostat along with the integration algorithm has to work harder to achieve a steady state. The GW integrator showed a deviation of 10% in the temperature (not shown) in the NEDPD simulations compared to the 2% deviation shown by the SCVV, S1, S2, and SCPHF integrators. For low friction simulations, both the NEDPD and SACF are viable methods for calculating the shear viscosity. However, as the friction increases, the NEDPD simulations involve higher uncertainties compared to the SACF simulations and in the GW case, a large deviation from the temperature. One possible reason for the large errors could also be the value of the shear rate imposed. However, we found that external velocities smaller than 0.5 at the boundaries did not give a good linear velocity profile. Hence, NEDPD would be most effective in an intermediate region where the shear rate is low enough to not adversely affect the thermostat and high enough to ensure a good velocity gradient in the system.

G. DISCUSSION

Based on computational efficiency, clearly the GW scheme stands out as the best. The temperature conservation properties of the SCPHF and Shardlow schemes are better than the other algorithms, which has been independently confirmed by our studies and other ones earlier [11,16,18]. With respect to the autocorrelation decay and transport properties, all the integrators perform in very similar ways at low friction and small time steps. Even when the time step is increased at low friction, there are negligible differences in the transport coefficients. The velocity autocorrelation decays exponentially for all integration schemes and the stress autocorrelation is almost identical.

For each autocorrelation function, three of the integrators matched very well and others showed some differences. The

SCPHF, S1, and S2 are closest to each other for VACF, and the SCVV comes very close. The SCVV, S1, and S2 are closest to each other for SACF, with the zero time values for SCPHF being high and GW being higher. The Shardlow S1 and S2 schemes have the lowest zero stress values.

At high friction limits and time steps of 0.04, the GW scheme breaks down. This is also known from previous work. All the other integrators show almost identical velocity autocorrelation decays. The SCPHF scheme shows a higher zero stress autocorrelation value compared to other schemes and smaller friction cases. The SCVV and Shardlow schemes again show identical decay profiles. The zero stress autocorrelation value is slightly higher for the SCVV scheme compared to the smaller friction values but remains unchanged for the Shardlow integrators. The diffusion constant shows little change between the integration schemes. Based on the VACF decay profiles and the diffusion constant calculations, any of the integration schemes can be used except the GW scheme at high friction, large time step limits. The shear viscosity on the other hand shows a lot of variation between integrators as seen in Fig. 3. The Green-Kubo and NEDPD results match reasonably well for the shear viscosity results and it may be valid, at least for the conditions simulated here, although extensive investigations of the validity are beyond the scope of this paper. With the high uncertainties though, the shear viscosity calculations seem to fall with the theoretical predictions.

H. CONCLUSIONS

Velocity autocorrelation decay, stress autocorrelation decay, diffusion coefficient, and shear viscosity were calculated in DPD. A parametric study using three different time steps, three different friction values, and five different integrators was performed. The velocity autocorrelation decay is exponential at low friction and short times, and deviates from exponential behavior at long times. At high friction, the deviation occurs more quickly and increases with time. The diffusion coefficient at low friction matches very well the existing theoretical predictions derived for low friction and low density. Deviation from these predictions occurs at larger friction values, as expected. Based on the VACF decay and diffusion constant results, any one of the integrators could be used for simulation purposes (except GW at higher friction and time step) as the deviations are not very significant. The stress autocorrelation decay is more rapid at high friction values compared to the low friction cases. At low friction, all the integrators show similar decay behavior, which changes significantly at high friction. The shear viscosity calculations were done using both Green-Kubo and nonequilibrium methods. Though the uncertainties are high, the shear viscosity falls within the range of well-predicted theories not only at low friction, low density, but also at high friction, low density.

ACKNOWLEDGMENT

This work was supported by the Office of Naval Research (Grant No. N00014-07-1-0665).

APPENDIX: NUMERICAL CALCULATION OF GREEN-KUBO INTEGRALS

The numerical integration of the correlation functions to calculate transport coefficients was done in MATLAB. The correlation curve was approximated using piecewise linear interpolation and the area was calculated using numerical integration.

In the case of diffusion coefficient, the integral in Eq. (27) was calculated at different time intervals of 1 DPD unit for 30 DPD units. The integral converged to a nearly constant value after a few time units as seen in Fig. 4. The diffusion coefficient is calculated as one third of the mean converged value. The standard deviation from the mean is shown in Table III. The standard error of the mean at each data point is approximately 10^{-6} and contributes to a constant error of 30 time units $\times 10^{-6}$ to the integral.

For shear viscosity, all integrals were calculated up to 100 DPD units. This corresponds to shorter time integration for smaller time steps and longer time integration for longer time

steps. For smaller time steps, better temporal resolution leads to larger fluctuations. Larger time steps result in smoothing of the fluctuations. Although the choice of 100 DPD units is arbitrary, we observe that the fluctuations in the data are higher for time intervals greater than 100 units. The error in the data increases with time because there are fewer time points available for longer time correlations, resulting in poorer statistics.

To calculate shear viscosity, the SACF [integrand of Eq. (29)] is calculated at each DPD time unit and fitted by piecewise linear functions. Integration of the piecewise functions is carried out up to 100 DPD time steps. Figure 4 shows the value of the integral for the first 100 time units. The value of the integral is chosen as the mean of the data averaged from 1 to 100 time units. The uncertainty is calculated as the standard deviation.

Using the mean value of the integral (Fig. 4), and multiplying by the factor $\bar{\Omega}/k_B T$ from Eq. (29), we get the shear viscosity for one particular case.

-
- [1] P. J. Hoogerbrugge and J. M. V. A. Koelman, *EPL* **19**, 155 (1992).
- [2] R. D. Groot, *Lect. Notes Phys.* **640**, 5 (2004).
- [3] P. Español and P. Warren, *EPL* **30**, 191 (1995).
- [4] C. A. Marsh, G. Backx, and M. H. Ernst, *Phys. Rev. E* **56**, 1676 (1997).
- [5] R. D. Groot and P. B. Warren, *J. Chem. Phys.* **107**, 4423 (1997).
- [6] A. Chaudhri and J. R. Lukes, *Int. J. Numer. Methods Fluids* **60**, 867 (2009).
- [7] T. Murtola, A. Bunker, I. Vattulainen, M. Deserno, and M. Karttunen, *Phys. Chem. Chem. Phys.* **11**, 1869 (2009).
- [8] C. A. Marsh and J. M. Yeomans, *EPL* **37**, 511 (1997).
- [9] J. B. Gibson, K. Chen, and S. Chynoweth, *Int. J. Mod. Phys. C* **10**, 241 (1999).
- [10] W. K. Den Otter and J. H. R. Clarke, *Int. J. Mod. Phys. C* **11**, 1179 (2000).
- [11] I. Pagonabarraga, M. H. J. Hagen, and D. Frenkel, *EPL* **42**, 377 (1998).
- [12] U. M. Ascher and L. R. Petzold, *Computer Methods for Ordinary Differential Equations and Differential-Algebraic Equations* (SIAM, Philadelphia, 1998).
- [13] P. E. Kloeden and E. Platen, *Numerical Solution of Stochastic Differential Equations*, *Stochastic Modelling and Applied Probability* Vol. 23 (Springer, New York, 1999).
- [14] G. Besold, I. Vattulainen, M. Karttunen, and J. M. Polson, *Phys. Rev. E* **62**, R7611 (2000).
- [15] I. Vattulainen, M. Karttunen, G. Besold, and J. M. Polson, *J. Chem. Phys.* **116**, 3967 (2002).
- [16] P. Nikunen, M. Karttunen, and I. Vattulainen, *Comput. Phys. Commun.* **153**, 407 (2003).
- [17] G. De Fabritiis, M. Serrano, P. Español, and P. V. Coveney, *Physica A* **361**, 429 (2006).
- [18] T. Shardlow, *SIAM J. Sci. Comput. (USA)* **24**, 1267 (2003).
- [19] M. Serrano, G. De Fabritiis, P. Español, and P. V. Coveney, *Math. Comput. Simul.* **72**, 190 (2006).
- [20] F. Thalmann and J. Farago, *J. Chem. Phys.* **127**, 124109 (2007).
- [21] C. P. Lowe, *EPL* **47**, 145 (1999).
- [22] E. A. J. F. Peters, *EPL* **66**, 311 (2004).
- [23] A. F. Jakobsen, G. Besold, and O. G. Mouritsen, *J. Chem. Phys.* **124**, 094104 (2006).
- [24] J. A. Backer, C. P. Lowe, H. C. J. Hoefsloot, and P. D. Iedema, *J. Chem. Phys.* **122**, 154503 (2005).
- [25] M. P. Allen and D. L. Tildesley, *Computer Simulation of Liquids* (Oxford Science Publications, Oxford, 1987).
- [26] D. Levesque and L. Verlet, *Phys. Rev. A* **2**, 2514 (1970).
- [27] D. Levesque, L. Verlet, and J. Kürkijarvi, *Phys. Rev. A* **7**, 1690 (1973).
- [28] W. G. Hoover, A. J. C. Ladd, R. B. Hickman, and B. L. Holian, *Phys. Rev. A* **21**, 1756 (1980).
- [29] D. M. Heyes, *Phys. Rev. B* **37**, 5677 (1988).
- [30] E. E. Keaveny, I. V. Pivkin, M. Maxey, and G. Em Karniadakis, *J. Chem. Phys.* **123**, 104107 (2005).
- [31] L. Verlet, *Phys. Rev.* **159**, 98 (1967).
- [32] S. Balay, K. Buschelman, W. D. Gropp, D. Kaushik, M. G. Knepley, L. C. McInnes, B. F. Smith, and H. Zhang, <http://www.mcs.anl.gov/petsc> (2001).
- [33] P. Español and M. Serrano, *Phys. Rev. E* **59**, 6340 (1999).
- [34] J. H. Irving and J. G. Kirkwood, *J. Chem. Phys.* **18**, 817 (1950).
- [35] M. H. Ernst and R. Brito, *EPL* **73**, 183 (2006).
- [36] D. J. Evans and G. P. Morriss, *Statistical Mechanics of Nonequilibrium Liquids* (Academic Press, New York, 1990), Chap. 4, p. 87.
- [37] M. H. Ernst and R. Brito, *Phys. Rev. E* **72**, 061102 (2005).
- [38] G. T. Evans, *J. Chem. Phys.* **110**, 1338 (1999).
- [39] A. J. Masters and P. B. Warren, *EPL* **48**, 1 (1999).
- [40] D. C. Visser, H. C. J. Hoefsloot, and P. D. Iedema, *J. Comput. Phys.* **205**, 626 (2005).
- [41] J. P. Hansen and I. R. McDonald, *Theory of Simple Liquids* (Academic Press, New York, 1976).